The Pennsylvania State University

The Graduate School

AN ANALYSIS OF PMT SIGNALS IN THE LZ DARK MATTER EXPERIMENT

A Thesis in

Physics

by

Gavin L. Cox

Submitted in Partial Fulfillments
of the Requirements
for the Degree of

Master of Science

December 2021

The thesis of Gavin Cox was reviewed and approved by the following:

Maria del Carmen Carmona Benitez
Assistant Professor of Physics
Thesis Co-Advisor

Luiz de Viveiros
Assistant Professor of Physics
Thesis Co-Advisor

Richard W. Robinett
Professor of Physics
Associate Head for Undergraduate and Graduate Students

ABSTRACT

Dark matter has become one of the longest standing mysteries in physics. The main idea behind dark matter is simple: on the largest of scales, luminous matter cannot account for the observed motion and clustering of galaxies and clusters of galaxies. Some unseen object, particle or force with the ability to interact gravitationally must be present throughout the universe to explain these observations. Since it was first hypothesized in 1933, some progress has been made to improve our understanding of this mystery. The indirect evidence indicating the existence of dark matter is extensive and gives many clues as to possible composition and distribution. LZ is an experiment whose goal is to finally observe the existence of dark matter through direct detection.

TABLE OF CONTENTS

List of Figures **v**

Acknowledgements **vi**

Indirect Evidence of Dark Matter **1**

Dark Matter Candidates **4**

Modified Newtonian Dynamics (MOND): 4

Massive Compact Halo Objects (MACHOs): 5

Axions: 5

Weakly Interacting Massive Particles (WIMPs): 5

LZ Experiment **6**

PMTs, Electronics and Data Acquisition **11**

Comparing the High Gain and Low Gain PMT Channels **15**

Energy Threshold for LG 24

The Future of LZ **26**

References **27**

LIST OF FIGURES

1. Galactic Velocity Distribution……...……2
2. Bullet Cluster……..……..3
3. CMB Power Spectrum……..4
4. LZ Experimental Setup……8
5. ER and NR Spectrum……....9
6. PMT Schematic……...12
7. Pulse Shaping in the Amplifiers……13
8. LZ's Electronics Chain……...14
9. HG vs LG of one PMT…….....15
10. Slopes of Unsaturated Pulses……..16
11. Slopes of Saturated Pulses……..17
12. HG Pulse Area Inflection Point……..18
13. Inflection Point Example……....18
14. Multiple Inflection Points……...20
15. Waveforms of Different Saturation Populations……21
16. Waveforms of Bottom Array Saturated Pulses……...23
17. Energy Threshold of LG……24
18. LG Pulses with no HG……...……25
19. Problems with the Pulse Finder……..25
20. Atypical Example of Misclassifying a Pulse……..26

Acknowledgements

I would like to thank my research advisors Carmen Carmona and Luiz de Viveiros for their help and guidance throughout my graduate career at Penn State. This work would not have been possible without their input. My future career is directly due to their support and encouragement, and I thank them for the opportunities that will present themselves for many years to come.

Funding for this work is supported by the U.S. Department of Energy, Office of Science, Office of High Energy Physics under DE-SC0019066. While this document is believed to contain correct information, neither the United States Government nor any agency thereof, nor any of their employees, makes any warranty, express or implied, or assumes any legal responsibility for the accuracy, completeness, or usefulness of any information, apparatus, product, or process disclosed, or represents that its use would not infringe privately owned rights. The views and opinions of authors expressed herein do not necessarily state or reflect those of the United States Government or any agency thereof.

Indirect Evidence of Dark Matter

Fritz Zwicky performed a study of the redshift of various extragalactic nebulae to determine their velocity dispersions [1]. Specific interest was given to the Coma cluster. This cluster has nebulae that have velocity differences of at least 1500 km/s. By plugging in the mass of all the visible matter into the virial theorem, Zwicky was able to conclude that this mass could not account for the large velocity dispersion. He estimated that the actual density must be 400 times greater than that of luminous matter. Despite this large overestimation, Zwicky was the first to predict that dark matter was responsible for this observational discrepancy.

Zwicky was able to provide evidence for the existence of dark matter, but its distribution was not well established until Vera Rubin presented her work on the velocity distribution within galaxies [2]. Using Newtonian gravity, one can predict the distribution of velocities versus radial position for the stars within a galaxy. As seen in Figure 1, the velocity of matter at large radii is much greater than that predicted using the distribution of visible matter in the galaxy. This observation necessitates that dark matter must be distributed throughout the galaxy rather than a large mass in the center. One such model that can explain this observation is the Standard Halo Model (SHM), which predicts an isotropic and spherically symmetric distribution of dark matter throughout the galaxy.

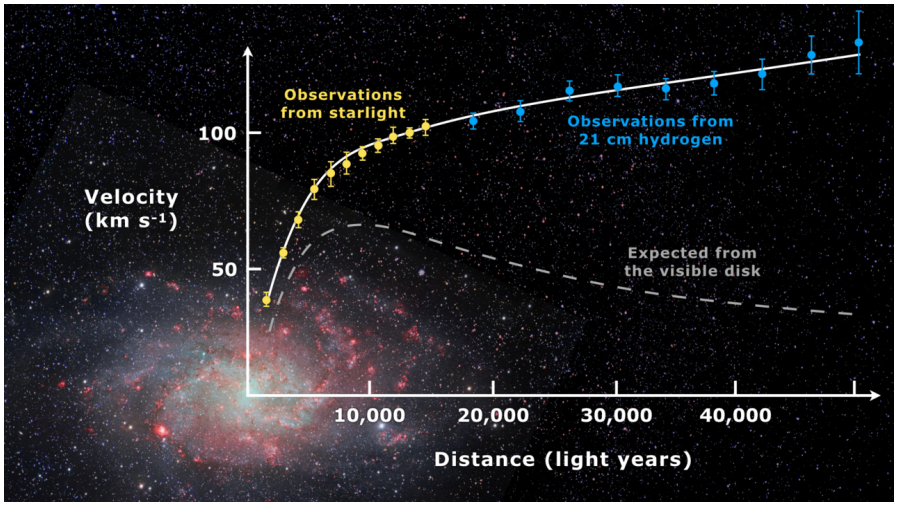

Figure 1: Velocity as a function of radius in a galaxy. The dashed line represents the expected velocity given the mass distribution seen from visible matter, whereas the observed velocity continues to increase far from the center of the galaxy. One possible explanation is that a halo of "dark" or unseen matter exists far beyond that of visible matter. [3]

Another breakthrough came through observations made in the Bullet cluster [4]. The Bullet cluster consists of two galactic clusters that have collided with each other in the past leaving both in a disrupted state. This collision gives a unique chance to see if the total mass distribution matches the distribution of baryonic matter. The two observations are made using gravitational lensing and X-ray spectroscopy, respectively. The result is a very significant separation between the two different distributions. The baryonic matter (dominated by gas) has interacted during the collision to produce an obvious bow shock on one of the clusters. However, the distribution of the majority of the mass of the cluster appears to be unaffected by the collision and retains its spherical shape. This seems to imply that the majority of the matter did not interact during the collision, but rather passed straight through. The Bullet cluster serves as great evidence that dark matter is primarily made of an unseen substance rather than a modification to the theory of gravity.

Figure 2: The Bullet Cluster. The figure shows an obvious disconnect between the X-ray spectrum (pink) and the gravitational influence (blue). Despite the collision, the spherical structure of gravity was not disrupted. [5]

Lastly, the cosmic microwave background (CMB) power spectrum provides one of the most compelling arguments for dark matter. Baryonic density and total matter density can be calculated directly through the analysis of the CMB, giving an estimate of non-baryonic dark matter [6]. After the Big Bang, the universe was in a radiation-dominated state. After the universe expanded, these overdensities can be seen as peaks within the power spectrum, giving a precise way to measure the relative density of normal matter. By finding the ratio of heights of even and odd peaks, the relative amount of baryonic matter in the universe has been calculated to be $\Omega_b = 0.0499 \pm 0.0002$. Dark matter would contribute to the gravitational attraction but would not self-interact like baryons. This difference allows for a measurement of the ratio between normal matter and dark matter. The Λ-CDM model (a model that assumes a combination of dark energy and dark matter) matches the observed power spectrum very well at nearly all angular resolutions. This measurement found the total matter density to be $\Omega_m = 0.315 \pm 0.007$. Therefore, the conclusion of this measurement is that dark matter is five times as abundant as regular matter. All of these measurements point towards the existence of dark matter, but only give a few clues as to its composition.

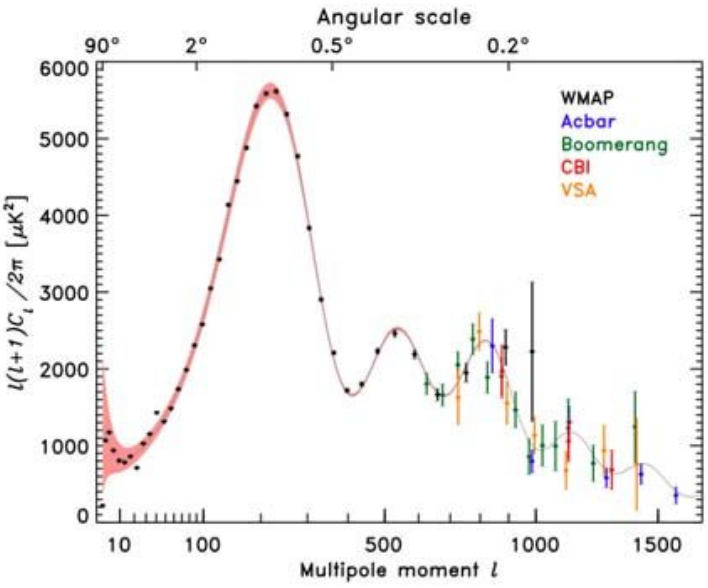

Figure 3: The measurement of cosmic microwave background power spectrum by many different experiments. The best fit of this data is produced by the Λ-CDM model, which incorporates dark matter and dark energy. The best fit model predicts that the abundance of dark matter is five times that of regular matter. [7]

Dark Matter Candidates

Since dark matter has been a popular area of study for a significant amount of time, many different models have been proposed. I will look at a few of the more popular candidates.

Modified Newtonian Dynamics (MOND):

This hypothesis assumes that the problem lies within our understanding of gravity on a large scale, rather than trying to posit the existence of new particles. By changing gravity to a function that decays slower than an inverse-square, the observed motion of galaxies could be explained. While this model shows potential for a typical galaxy, it cannot explain how the Bullet cluster shows a disconnect between baryonic mass and center of gravity. If MOND does turn out to be correct, it can only account for a fraction of dark matter.

Massive Compact Halo Objects (MACHOs):

This hypothesis considers the possibility that dark matter is made up of very large, massive objects that do not emit any light, such as brown dwarfs, black holes, or neutron stars. If these objects were scattered throughout the galaxy in a halo, they could be responsible for dark matter. These objects can be detected through surveys analysing the microlensing of stars when a massive object passes in front of it. The results of these surveys seem to indicate that MACHOs only make up ~1% of dark matter. Despite being a promising candidate, we must look to other potential theories.

Axions:

CP violation is another long-standing problem in physics. For a long time, CP symmetry was assumed to hold for all interactions since no counterexamples had been produced. Then in 1964, Cronin and Fitch discovered that kaons exhibited indirect CP-violation, which in turn led to their Nobel Prize in 1980. Direct CP-violation was also seen in kaons in the late 1990s, further cementing its existence. But the reason for the near symmetry in almost all particle interactions continues to be a mystery. One solution put forth by Roberto Peccei and Helen Quinn postulates that this suppression is caused by a new field, in which a Goldstone boson can arise. This extremely light boson is called an axion. If the axion density in the universe was large enough, this particle could make up dark matter. This hypothesis is attractive because two fundamental mysteries could be solved with the discovery of the axion. [8]

Weakly Interacting Massive Particles (WIMPs):

One of the most compelling hypotheses for dark matter are WIMPs. These hypothetical particles have mass on the order of 10 GeV - 1 TeV, a small cross-section and are electrically neutral. If WIMPs are distributed throughout galaxies in a halo, they would explain why Rubin’s velocity curve flattens at large radii. Their presence in the early universe would explain the power spectrum of the CMB and the

predicted ratio of matter to dark matter. And critically, they would be able to explain the separation of gravity and baryonic matter in the Bullet cluster. Since dark matter is assumed to rarely interact with all matter, regular or dark, the WIMPs in each cluster were able to pass right through each other and maintain their spherical shape. This ability for WIMPs to explain all of these phenomena makes them the favorite candidate to date.

The evidence for WIMPs does not stop at observational evidence of dark matter; particle physics also predicts a particle with characteristics very similar to a WIMP. The “WIMP Miracle” is a derivation employing thermal freeze-out of particles near the beginning of the universe. In the very early universe, the production and annihilation of dark matter particles would reach an equilibrium due to the density and energy of the universe. As the universe expanded, the production rate would slow. Eventually, the expansion rate would become so great that the annihilation rate would also slow, leaving the dark matter density we observe today. This freeze-out density can be calculated based on the initial particles characteristics. Using this method, one will find that the observed density of dark matter can be reproduced by a particle with mass on the order of the weak scale: 100 GeV to 1 TeV. While this coincidence is not proof for the existence of dark matter, it does make the theory more convincing and worthy of further research. LZ is one of many experiments dedicated to continuing the hunt for this elusive particle and will, at the very least, increase our knowledge of the WIMP parameter space.

LZ Experiment

The LZ experiment is located in Lead, SD, at the Sanford Underground Research Facility (SURF), which is the former Homestake gold mine, at about one mile underground (4850' level). The large amount of rock above provides great shielding from cosmic rays. The removal of this background plays a large part in achieving the high sensitivity necessary to detect the signal from a WIMP interaction in the detector. The main part of the detector is a time projection chamber (TPC) with a large amount of xenon as the target mass: LZ will be using 10 tons of xenon in the experiment, 7 of which will be located

in the active region of the TPC [9]. Gammas and neutrons generally have a small mean free path in xenon, allowing for a desirable self-shielding effect that allows the center of the xenon to have less background than the outer edges. To take advantage of this property, we define a smaller volume at the center of the xenon, called the fiducial volume. This fiducial volume is the region where our WIMP search analysis will take place. Another way to mitigate backgrounds is through a veto. LZ will implement a veto system composed of three parts: the Xenon Skin, the Outer Detector (OD), and the water tank. These elements can be seen in Figure 4. The Skin will be 4-8cm of xenon located outside the walls of the TPC and on the bottom dome. A major background that will be seen in this region is gamma events that scatter once in the TPC before escaping. The OD will be located outside of the cryostat which houses the TPC, shown in green in Figure 4. It is made of a gadolinium-based liquid scintillator that is very good at tagging neutrons. Since neutrons interact with xenon in the same way as WIMPs, vetoing these events is very important. The water tank houses the entire detector, including the OD. Over 200 tons of water will be useful in shielding against external backgrounds coming from the shotcrete that covers the entire cavern. Events that scatter once in the TPC before escaping have a chance of replicating a WIMP signal. Therefore, this veto system plays a large role in improving the sensitivity of the detector and raising our confidence that a detected WIMP signal is legitimate.

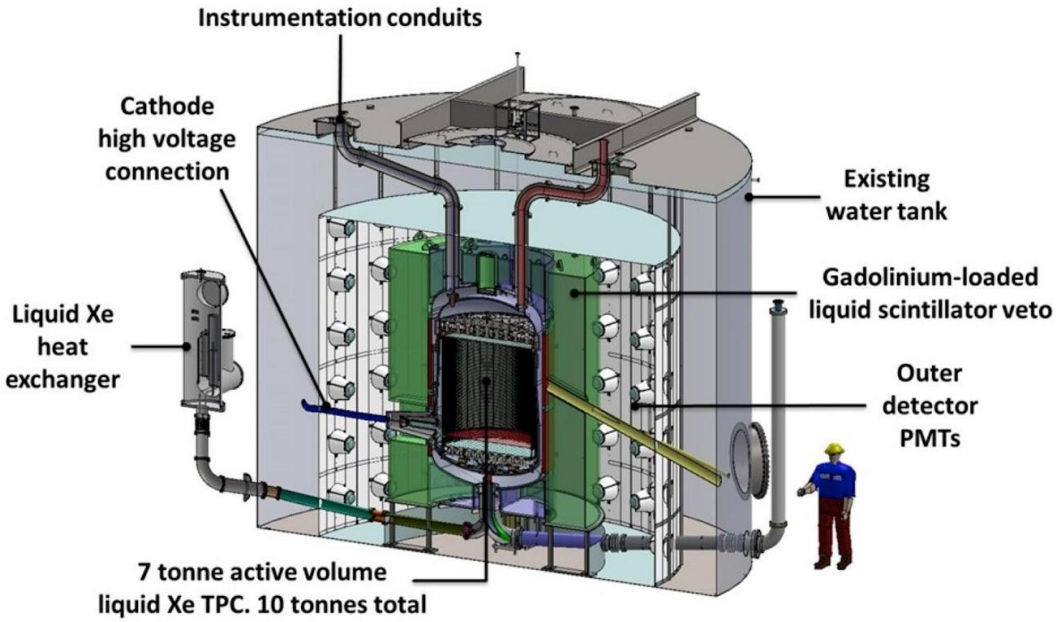

Figure 4: The experimental setup of LZ. The TPC at the center houses seven tons of liquid xenon. The OD (green) is hermetically sealed around the cryostat. The PMT system for the OD and water tank (white) is outside this detector. This is all located within a 228-ton water tank. [10]

When an event occurs in the TPC, two different types of signals are created: scintillation and ionization. The scintillation light is seen directly by the photomultipliers (PMTs) and it is called the S1 signal. Due to reflection off of the liquid surface at the top of the detector, the S1 signal is mainly seen in the bottom array of the PMTs. The ionization signal, called S2, is seen by detecting the electrons emitted after an interaction. A large electric field of 310 V/cm is applied throughout the length of the active volume to drift the electrons away from the newly produced Xe ion and towards the top of the TPC where we have an interface of gaseous and liquid Xe. A high voltage applied across the liquid-gas boundary extracts the electrons into the gas, which then produces light via electroluminescence that will also be seen by the PMTs, producing the S2 signal. The S2 is a much larger signal in comparison to the S1. The TPC detector has an excellent 3D position reconstruction within ~1cm. The relative time separation between the S1 and S2 signals gives the interaction z-coordinate (since electrons take time to drift upwards), and the hit pattern of the S2 signal on the PMTs gives the (x,y) coordinates. All analyses are primarily based on these two signals and their structure (size, width, etc.).

WIMPs are expected to be neutral particles, thus we expect them to interact as a nuclear recoil (NR) with a Xe nucleus. This is in contrast with most of our backgrounds which will scatter off electrons, producing an electronic recoil (ER). The key difference between these two interactions is the ratio of ionized electrons (S2 signal) to scintillated photons (S1 signal). An ER will ionize more electrons by nature of the interaction, which will create separate bands of ER events and of NR events when we plot S1 vs log(S2/S1) (see Figure 5). The ER events (blue) are located higher in the parameter space than the NR events (orange), allowing us to reject ER events. In LZ we will have an ER background rejection efficiency of 99.5%, and we can define our region of interest to find WIMPs below the mean of the NR band. It should be noted that this quoted efficiency is only a "figure of merit" based on simple "cut-and-count" analysis techniques, and LZ will instead use Profile Likelihood techniques to identify and determine the significance of signals over backgrounds.

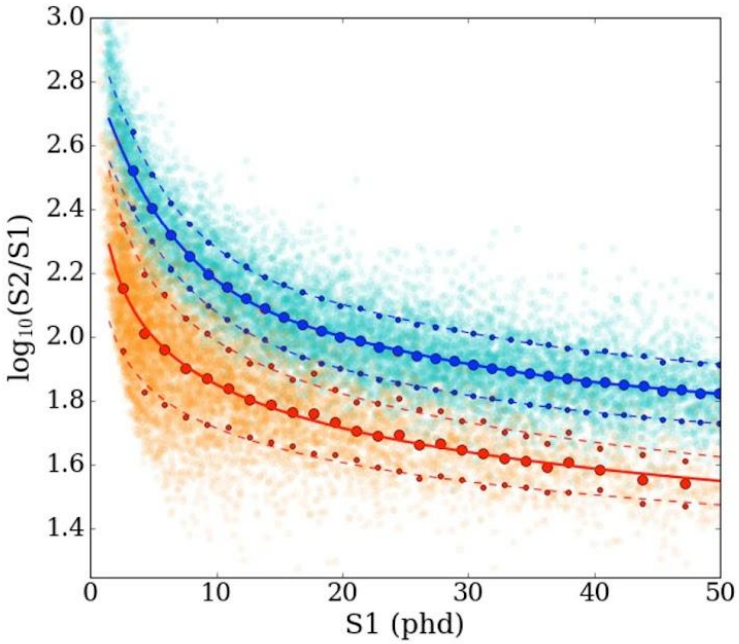

Figure 5: Calibration measurements of the ER (blue) and NR (orange) spectrum in the LUX experiment, LZ's predecessor using the same liquid xenon TPC technology. The separation of the ER and NR bands will be the basis for removal of a majority of LZ's backgrounds. [10]

One of the challenges of having such a sensitive detector is the many sources of backgrounds that will have to be considered and mitigated. Some backgrounds can be directly blocked from reaching our

detector. For instance, by locating our detector deep underground, cosmic rays become a sub-dominant source. However, many of our backgrounds are intrinsic to the detector itself and cannot be directly removed. These would include radioactive isotopes of detector materials, other noble gases mixed with the xenon and cosmogenic activation of xenon on the surface. In order to mitigate the backgrounds from detector materials, we had an extensive radioassay campaign, screening all the materials before they were used in the detector [11]. For example, our cryostat is made of titanium, which naturally contains radioactive ^{238}U, ^{232}Th, and ^{40}K, so great effort was made to identify titanium as radio-pure as possible to make the cryostat [11]. Another important radioactive background is Radon (^{222}Rn and ^{220}Rn), which can be found mixed with the Xenon. Radon from the air also plates out on surfaces, so in order to mitigate this background the construction of the detector was done in a reduced radon cleanroom, and we also performed Radon emanation measurements from the main detector components and the xenon circulation system. In our circulation system, we have a commercial getter that can remove the non-noble elements from the Xenon. However, it cannot remove noble elements, such as Ar, Rn, and Kr, and radioactive isotopes of Xe. Therefore, we will clean our Xenon before we put it inside the detector, using a chromatography-based system which removes the Krypton below the LZ design requirements (less than 0.3 ppt g ^{nat}Kr / g Xe). However, cosmogenically activated Xenon, such as ^{127}Xe, cannot be removed before bringing the xenon underground. Our method of removing this background is simply waiting for it to decay. With a half-life of 36.2 days, ^{127}Xe will be a significant background at the start of the run, but will become much less substantial over the 1000 live-days. When combining all of these background sources together, we can get an estimate of the number of ER and NR signals that will be in our region of interest over the full run. After applying 99.5% ER background rejection and 50% NR efficiency, we expect about 5.66 ER events and 0.52 NR events over the 5600 ton-live-days (1000 live-days with a 5.6 ton fiducial volume) [12].

To effectively model these backgrounds, the detector needs to be properly calibrated to ensure we understand the energy spectrum and resolution. LZ has an inherent challenge with calibration because of the self-shielding property of xenon. Typically this is an advantage since most backgrounds will interact

before reaching the fiducial volume. However, this also means that any calibration source placed outside of the detector would not reach the center of the xenon. This requires a method of injecting sources into the detector and removing them before data acquisition begins. The sources would necessarily have a short half-life or be able to be removed by the getter so they will not be present during the science run. Injecting these internal sources then removing them has been demonstrated previously in LUX.

For position reconstruction ^{83m}Kr and ^{131}Xe will be used due to the former's monoenergetic peak and the latter's high energy. These sources will be using a common injection method of flowing xenon gas over the source to carry it into the detector. Internal calibration sources include tritiated methane to measure low energy ERs throughout the detector and ^{220}Rn whose daughters will accumulate on walls and other surfaces allowing for calibration in these more complex locations [13].

Not all calibration sources will have to be injected into the xenon to perform properly. Neutron and gamma sources will be placed just outside the detector in a dedicated source tube. Multiple neutron sources will be used to cover a range of energies, including a deuterium-deuterium (DD) neutron generator and AmLi. The gamma sources, such as ^{228}Th, are not meant to penetrate into the fiducial volume, but instead will be used to calibrate the Xenon Skin and the OD vetoes. By using a large spectrum of calibration sources, LZ is confident in its ability to reconstruct the energy of both ER and NR events. These calibrations are necessary to ensure that the background and signal models used in calculating the sensitivity accurately represent real events.

PMTs, Electronics and Data Acquisition

LZ will be an extremely low background experiment designed to observe a rare NR of a WIMP off of a Xe nucleus. Because these events are so infrequent and only produce a small amount of light and a few electrons, a sensitive instrument is required. The typical instrument used in this type of experiment is the photomultiplier tube (PMT). Figure 6 shows a schematic of a typical PMT. Light is incident on the photocathode, which will produce an electron via the photoelectric effect. A PMT will have a high

voltage supply that is fed into a gradient from the photocathode to the anode along dynodes. When a photoelectron accelerates then hits the first dynode, a cascade of electrons are then emitted. These electrons are then accelerated to hit the second dynode, which then emits an even larger cascade of electrons. This amplification continues until the electrons reach the anode and a detectable output signal is generated.

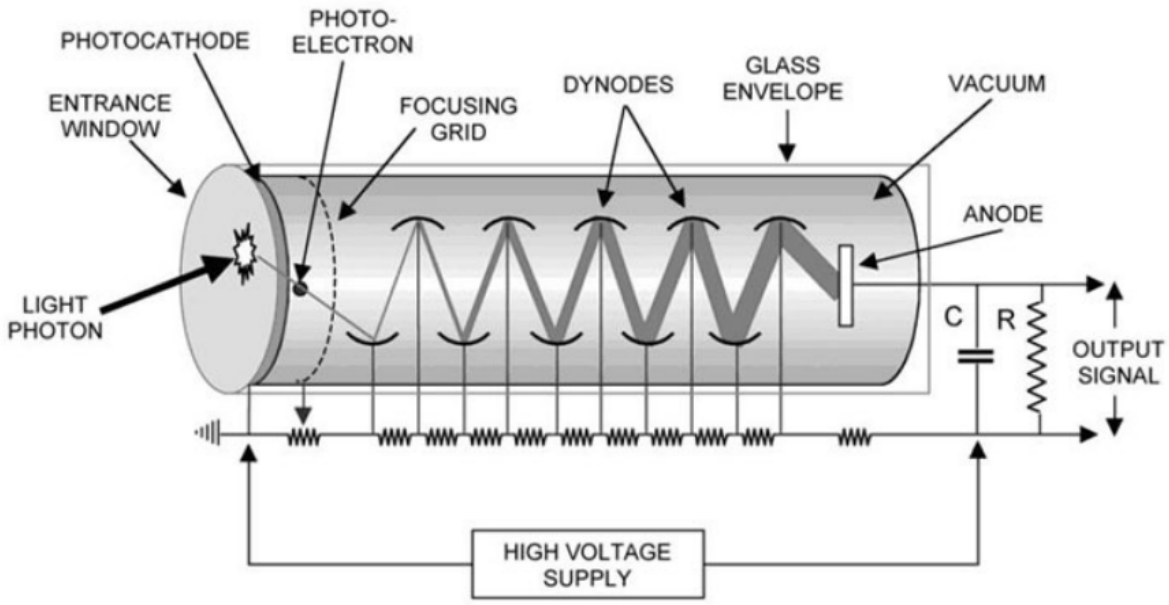

Figure 6: A schematic showing how a typical PMT produces a detectable signal from an incident photon. The photon first produces a photoelectron within the photocathode. This electron is then accelerated to the first dynode by the HV supply. When the electron hits the dynode, a cascade of electrons is produced. This amplification is replicated until a large enough signal reaches the anode, creating the output signal. [14]

The TPC contains a total of 494 3-inch Hamamatsu PMTs with high quantum efficiency optimized for typical S1 and S2 vacuum ultraviolet (VUV) wavelengths. These PMTs underwent a large campaign to ensure they can be operated in LXe and to prevent introducing a large amount of background radiation. The standard characteristics analyzed in this campaign were after-pulsing, gain, single photoelectron resolution, dark rate count and linearity to ensure all PMTs meet expectations. After these characteristics were measured at room temperature, they were again measured after a thermal cycling from 300 K to 160 K. Since the PMTs are located within the TPC, any radioactive materials will produce

a visible background throughout the duration of the experiment. Through collaboration with Hamamatsu and screening done by LZ, the radioactivity in the PMTs has been reduced ~1000 times compared to a similar model that has not gone through the screening. The signals from the PMTs also undergo scrutiny to ensure an identifiable pulse. The output of the PMTs are passed through an electronics chain containing custom amplifiers and are fed to the data acquisition system. The electronics are designed to have a >90% efficiency of detecting a single photoelectron. The gain and shaping parameters of the amplifiers are optimized to prevent saturation of the signal in the operating range. This range is defined by the S2 signal of the ^{131m}Xe 164 keV line. Calibration of the TPC PMTs will be done using LEDs situated in both the top and bottom array which allows operators to produce both single photoelectrons and afterpulsing.

One of the main problems with a raw signal from a PMT is the small amplitude and long tail. A small amplitude will prevent the pulse classifier from correctly identifying a pulse, and a long tail will cause more pile-up among signals due to increased pulse overlap. The amplifier is meant to amplify the signal while the shaping helps with the signal-to-noise ratio and prevents signals from overlapping. Figure 7 shows a simple illustration of a signal before and after it has been shaped. After being converted to a "bell-curve", the characteristics of the pulse are much easier to classify.

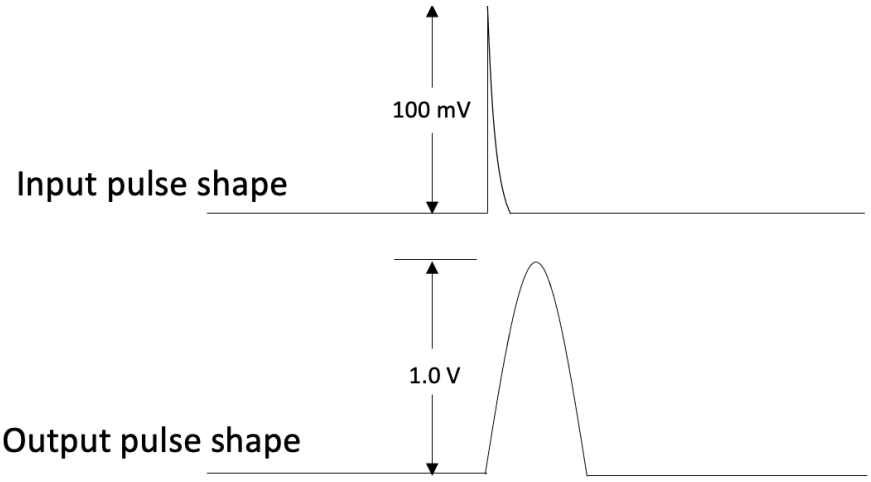

Figure 7 - A PMT signal typically has a long tail. After going through the amplifier, the signal will be amplified (from 100mV to 1.0V in this case) and also be shaped from the long tail into a more Gaussian peak. This increases the signal-to-noise ratio and reduces pile-up of signals.

The electronics chain for LZ is depicted in Figure 8. Signals from the PMTs leave the TPC through 'breakout boxes', which transition the cables from Xe space to cavern air. The analog signals are

then passed to two parallel paths or channels, one called High Gain (HG) and the other Low Gain (LG), they are amplified and shaped accordingly, and are digitized by the Data Acquisition system (DAQ). These digitized signals are then stored locally on disk. An improvement to the previous generation of LUX is the dual-gain amplification of the signals from the TPC PMTs. The HG amplifier has 60 ns full-width-at-tenth-maximum (FWTM) shaping and amplifies the area by 40 within that region, while the LG has 30 ns FWTM shaping and amplifies the area by 4 within that region. This difference allows the LZ signal processing software to potentially operate in a 'mixed gain' mode, where data is primarily read from the HG channels, but HG channels that have been saturated are replaced with their LG counterparts.

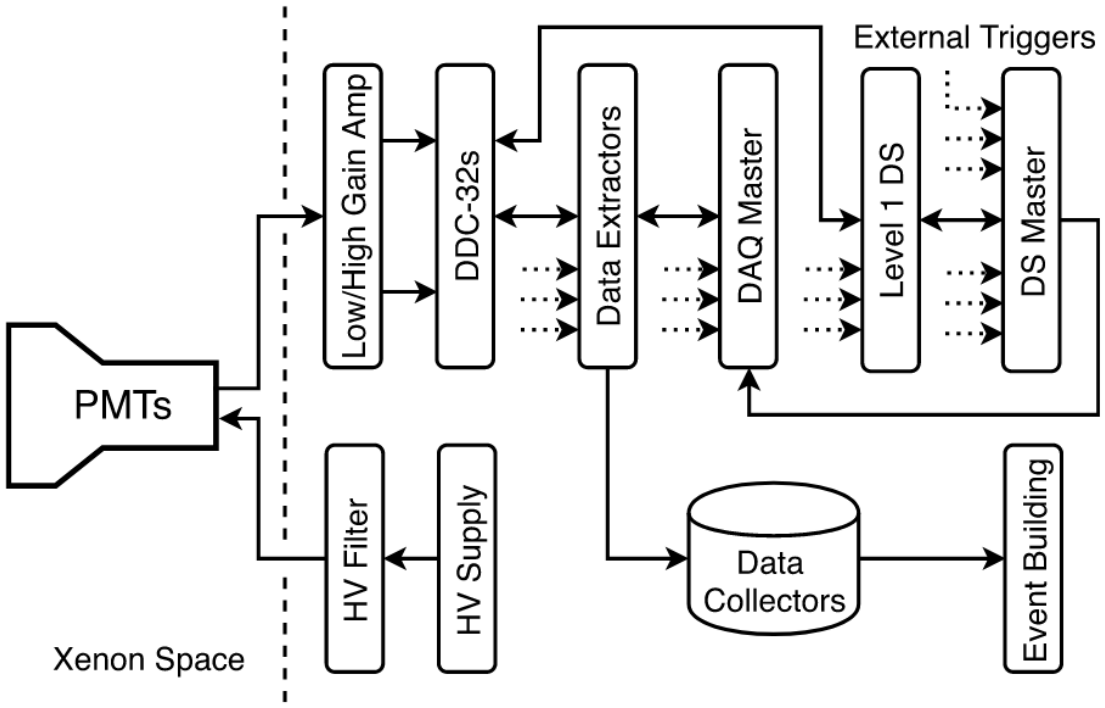

Figure 8: LZ electronics chain. An event which is incident on a PMT will be amplified through the HG/LG channels. It will then be routed through the Data Extractors to determine if it's an interesting signal. If so, it will be stored on the Data Collectors and will go through the process of Event Building. After this, it can then be analyzed through LZ's offline software. [10]

After the signal has been digitized and stored locally on disk, the Data Extractors will scan for interesting events which will then be compressed, stacked and temporarily stored on the Data Collector. The Event Builder then takes this data and organizes it into events that can then be analyzed through

online and offline means. A prototype of this full chain has already been tested and shown to detect single photoelectrons with an efficiency of 99.8%, exceeding the requirement of 90%.

Comparing the High Gain and Low Gain PMT Channels

LZ's PMTs have both High Gain (HG) and Low Gain (LG) channels to detect pulses within the detector. Most of the time, the HG channel will be used to process these observed pulses. However, for large pulses, such as S2s, the HG channel may become saturated which will cause a fraction of the pulse area to be lost. When this occurs, we would prefer to use the LG channel to have a better estimate of the pulse's true area. Therefore, we need an understanding of how the two channels relate to each other for the same pulse, whether saturated or not. The data used for this analysis was real gas data in the detector. Unfortunately, collecting both HG and LG data is resource intensive, so we only have a single successful run with both channels. Since a liquid boundary did not exist in the gas data, the PMT responses of all PMTs should be similar for events seen in the detector. Figure 9 shows a plot of the LG pulse area vs HG pulse area for PMT channel 15's unsaturated pulses, and compares the linear fit of the LG vs HG data(red-dashed) to a unit trendline y=x (black-dashed).

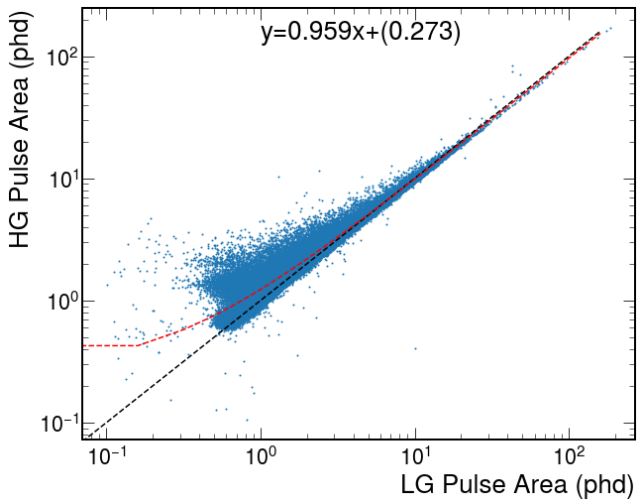

Figure 9: This data is a comparison of HG vs LG of unsaturated pulses for a single channel in the TPC. The trendline (red-dashed) for HG and LG pulse area of unsaturated pulses should have a slope close to one, which is demonstrated well by this channel. The trendline is a linear fit; the curve at low pulse areas is due to truncation error.

For nearly all channels in the detector, the slope for unsaturated pulses is close to one, showing good agreement between the two gains - see Figure 10. I have separated the slopes by whether the PMT is located in the top or bottom array. As expected, all slopes are approximately 1, which demonstrates a good relationship between the HG and LG channels. However, the top array has less variance than the bottom array, which could indicate a difference between the two arrays.

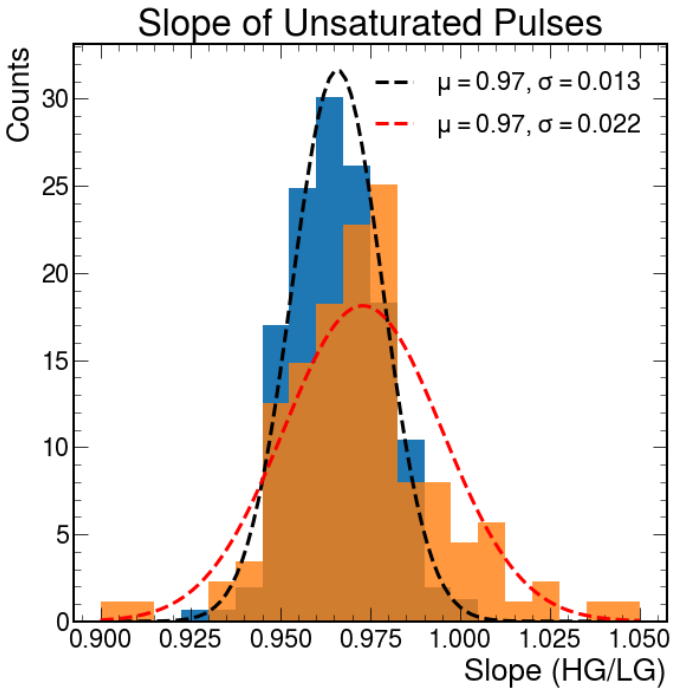

Figure 10: The area of unsaturated pulses in HG and LG should be equal, giving a relative slope of one (Figure 9). All the PMT channels in the TPC are plotted here and shown to have a slope close to 1. However, the bottom array (orange) has a greater variance than the top array, which hints that their pulse areas may be treated differently.

I then calculated the slope of saturated pulses using the same method used for unsaturated pulses. When a pulse is saturated, the HG channel will have less pulse area than the LG channel, so the expectation is that the slope of the trendline will be less than one. We can then use this information on a channel-by-channel basis to determine the energy at which each PMT will become saturated, at which point we will have to use LG instead of HG. This technique works very well for the top array, as seen in Figure 11. The slopes of nearly all PMTs in the top array change quickly and markedly, which allows the inflection point to be easily located. Figure 12 shows a histogram of the inflection points for the top and

bottom PMT arrays. These two figures illustrate that the bottom array has a different behavior than the top array. The saturated slopes of the bottom array are not drastically different from the unsaturated slopes. Since the slopes are close to parallel, their intersection can vary wildly and not give useful information such as when to use LG. Many channels in the bottom array have no obvious inflection point, having either a low number of saturated pulses or a large variance between HG and LG. Figure 13 illustrates this difference: two example channels from the top array and the bottom array. The goal is to find the intersection of the unsaturated slope (green-dashed) and saturated slope (red-dashed). Channel 15 from the top array shows an obvious change in slope, whereas channel 447 shows no visible change after pulses have been saturated. Another peculiarity shown in Figure 13 is the range of the saturated pulses. The bottom array sees much larger pulse areas than the top array despite viewing the same events without a liquid barrier. Again, the distribution of slopes for the saturated pulses for the bottom array are shown in Figure 11. However, we only include the channels with well behaved trendlines that cross the unsaturated pulse trendlines. This is why the number of channels in the bottom array appears to be far less than the top array.

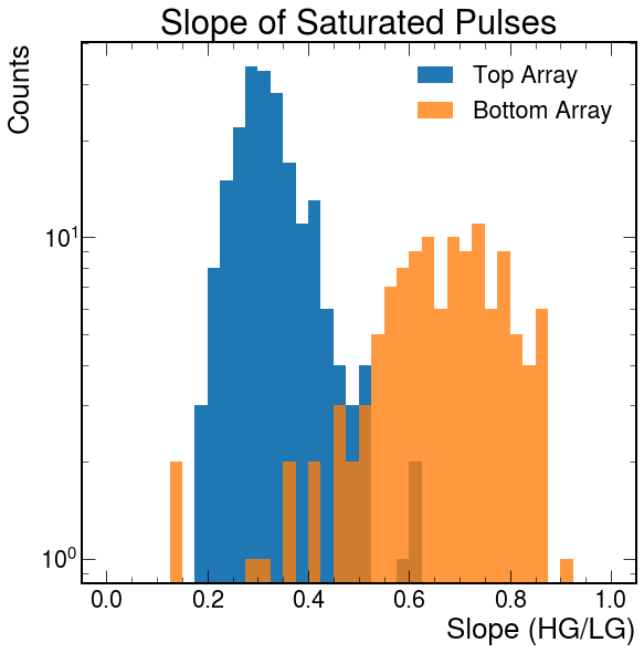

Figure 11: The same analysis was done for saturated pulses. Since the HG channel is saturated, some of that pulse area will be lost, causing the slope to fall below one. Here we can see a distinct difference between the top and bottom array which will affect the rest of my analysis.

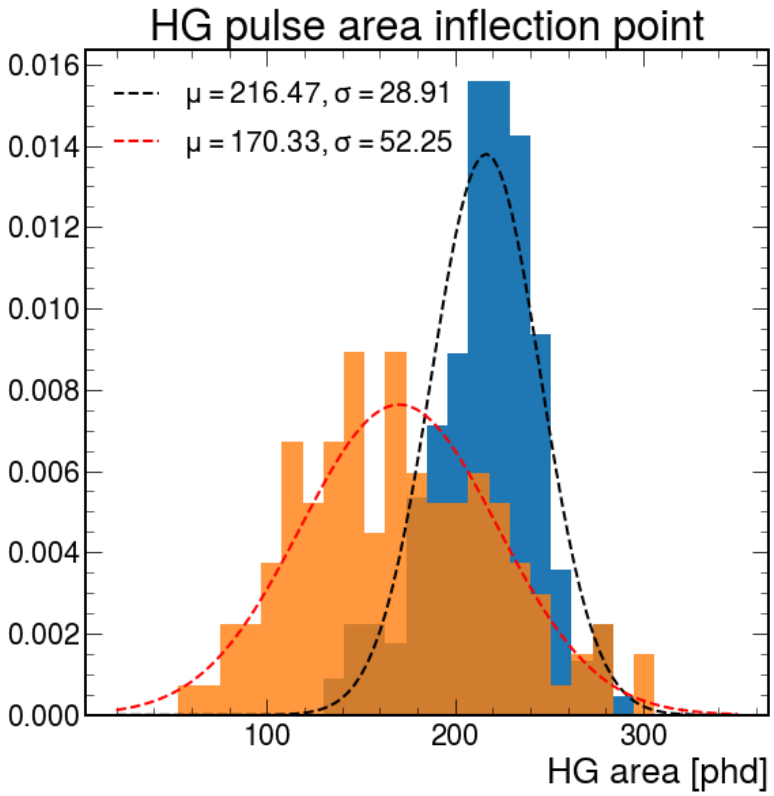

Figure 12: A histogram comparing the HG pulse area inflection points of the top array (blue) to the bottom array (orange). These points indicate the pulse area at which to switch from using HG to LG, since many of the pulses past this point will be saturated.

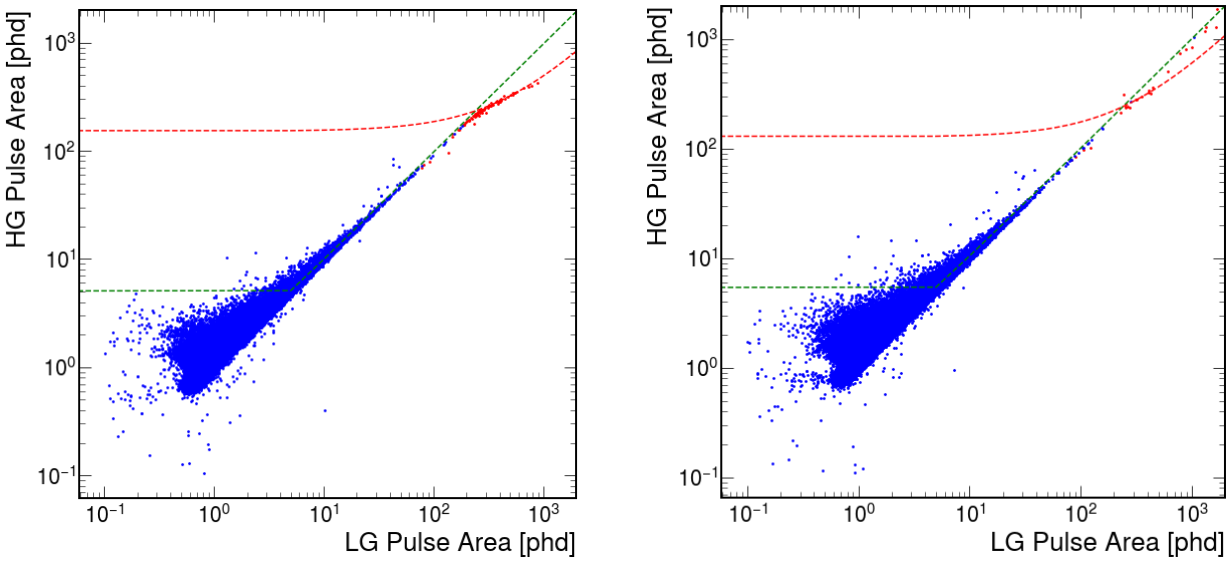

Figure 13: A typical example PMT from the top array (left) and bottom array (right) demonstrates the difference in slopes of saturated pulses (red-dashed). The top array's HG channel saturates and sees a reduced pulse area, whereas this is not the case for the bottom array. The bottom array also sees much larger pulses (>1000 phd) more regularly than the top array. This leads me to believe a correction is being applied to the top array but not to the bottom.

The HG-LG comparisons also highlighted a smaller population that falls off the y=x line faster than the majority of pulses. This is illustrated in Figure 14, showing channel 153, but note that this feature is seen in most top array PMTs and many bottom array PMTs. In order to draw conclusions about their inherent difference, an analysis of their waveforms must be made. Figure 15 highlights three different pulses with LG areas around 100 phd. Naively one may assume that whether a HG pulse saturates is dependent only on its pulse area. That does play a role, but its width is also a large determinant in whether it saturates. This is well illustrated using the three pulses that have roughly the same LG area. The unsaturated pulse not only has a large amplitude, but it also is very wide which will increase the pulse area. The saturated pulse closest to the unsaturated one maintains this similar shape: a large amplitude with a wide base. Most pulses in the gas data area are similar to these two shapes. The saturated pulse with the smallest HG area is a member of the population that saturates before most other pulses, and the waveform gives a good indication as to why. The pulse is very sharp, causing the PMT to quickly saturate and lose a large fraction of its pulse area. The topology of these events is consistent with interactions occurring very near the PMT faces, as the majority of the total pulse area will be contained in a single PMT. Since this population is evident in most PMTs, these sharp pulses are real signals and not a faulty PMT. When LXe data containing both HG and LG is successfully taken, checking to see if this population still exists will be an interesting task.

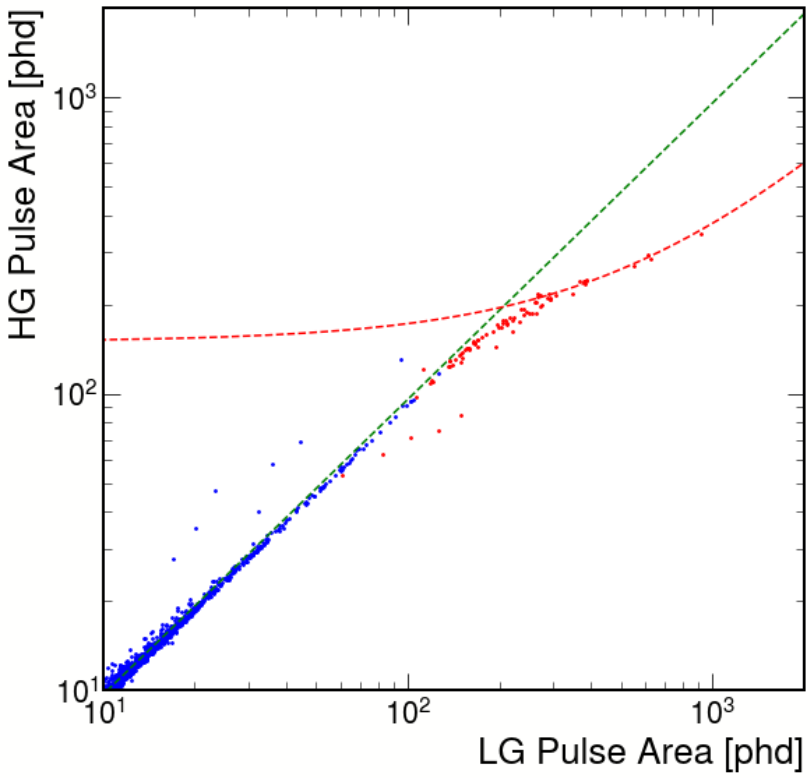

Figure 14: A typical channel that shows two different saturated populations: one where the red trendline is and another smaller one at lower energies. Since this smaller population is in most channels, a physical process must be causing it to saturate where the bulk of signals do not.

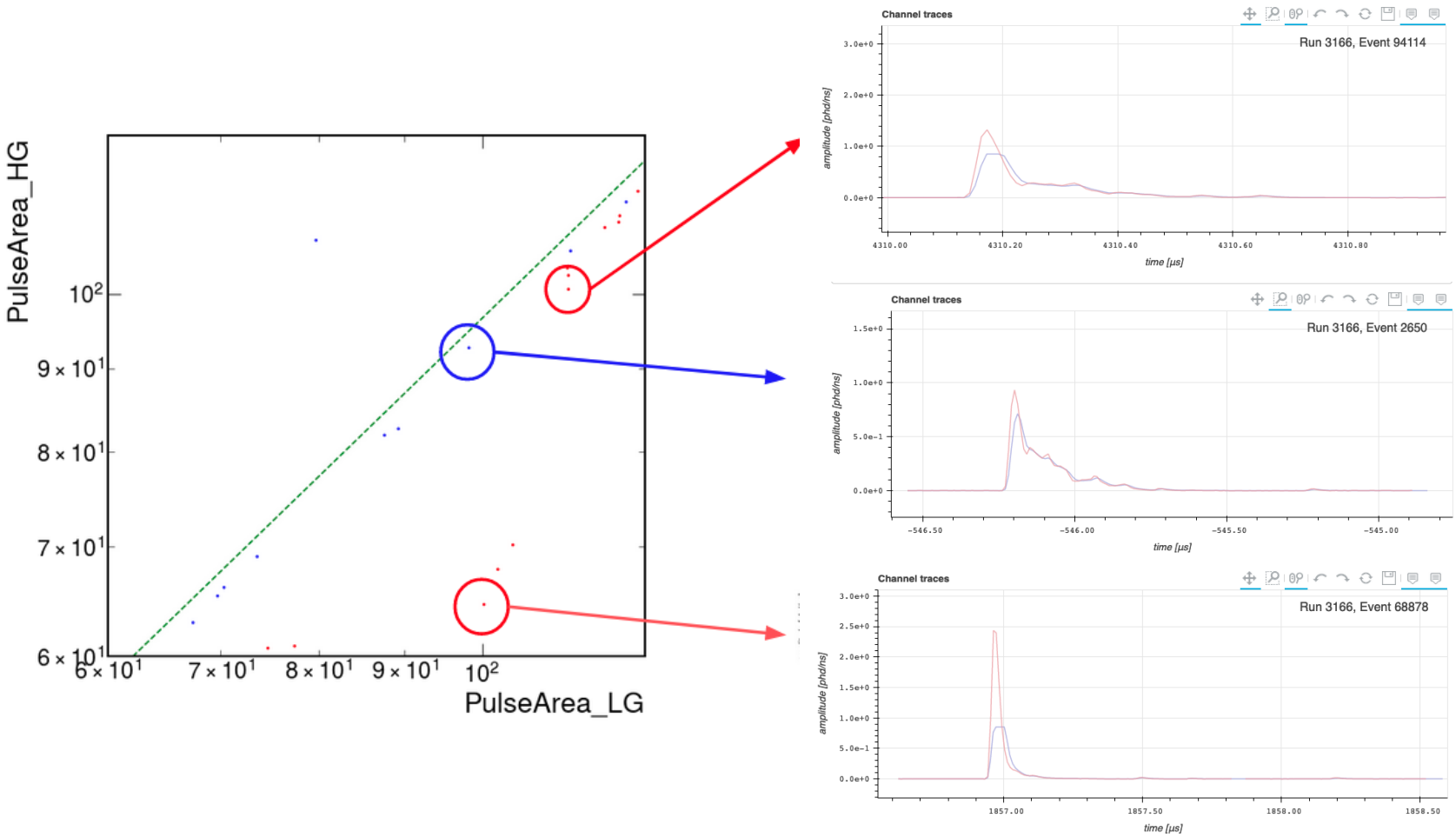

Figure 15: Using channel 153 from the top array, I analyzed three example waveforms with similar LG areas: one typical saturated pulse, one unsaturated pulse, and one saturated pulse from the smaller population. The first two have similar width and shape, whereas the third resembles a Delta function. This waveform has nearly all of its width in the saturated region, causing it to lose a larger fraction of HG pulse area compared to the others.

Hand-scanning waveforms also helps to better understand the differences seen between the top and bottom arrays. Since all PMTs in an array behave similarly, there is reason to believe some physical process or geometry is leading to different results. When looking at the largest pulses in a typical bottom array channel, the waveforms all have the same characteristics: large initial spike that slightly saturates which is followed by a long tail (see Figure 16). This waveform size and shape is consistent with the S2s that are expected to be seen in the gas region. We hypothesize that since the detector is all gas, these pulses are also "S2s", produced by the same physical process that produces S2 pulses when we operate in dual-phase mode. In the TPC beneath the cathode is a bottom grid intended for grounding when the detector is in full operation. When the PMTs are on, the PMT faces are held at some voltage to induce the amplification cascade necessary to see such small signals. This voltage creates an electric field between the bottom grid and the PMT faces, which might lead the electrons in this region to produce light via electroluminescence. While operating in gas, these large "S2-like" signals will be inevitable, but they should disappear once the detector is full of liquid.

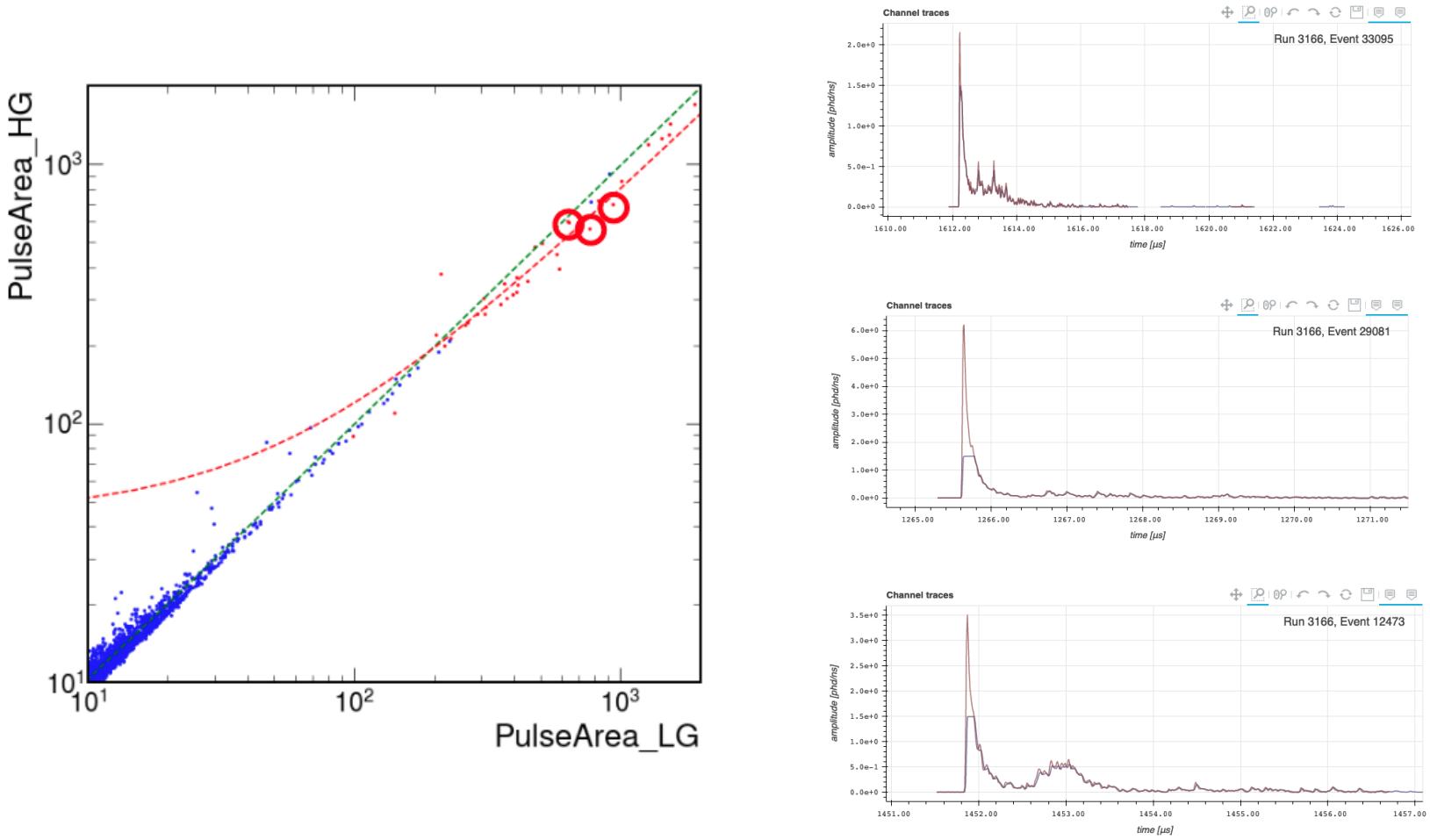

Figure 16: For bottom array PMTs, the saturated pulses had no obvious inflection point. By looking at the waveforms of pulses that had large pulse areas, these pulses had an initial spike that saturated but also had a large tail that added to the total pulse area. This is a signature of electroluminescence of electrons in Xe gas. Since the PMTs were biased, the TPC had an electric field between the unbiased bottom grid and the PMT faces, causing electrons in this region to act like an S2 signal.

Energy Threshold for LG

I also analyzed pulses that contained a HG signal but no LG signal. This would indicate that the pulse was too small to be seen in the LG channel. Looking at the pulse area distribution of the events with HG signal but not LG, we find a minimum LG pulse area of 0.5 phd (see Figure 17). The LZ analysis only uses LG pulses when HG saturates, so the lowest pulse area needed from the LG channel is 100 phd. Therefore, LZ does not have to worry about potentially missing a LG signal when the HG saturates. I also looked at the distribution of pulses that had LG but no HG (see Figure 18). These signals should not exist, because any pulse large enough to have a LG signal should certainly have a HG signal. By looking directly at these waveforms, the problem became obvious, shown in Figures 19 and 20. For a single pulse in HG, sometimes our waveform processing software will treat that same pulse as two or more pulses in LG. While one of those LG pulses will be associated with the original HG pulse, the others will not have a partnering HG pulse. Figure 20 shows an extreme example of this defect: a single HG pulse was seen as more than 1600 LG pulses. LZ's pulse-finder will need to fix these bugs for future analysis between HG and LG.

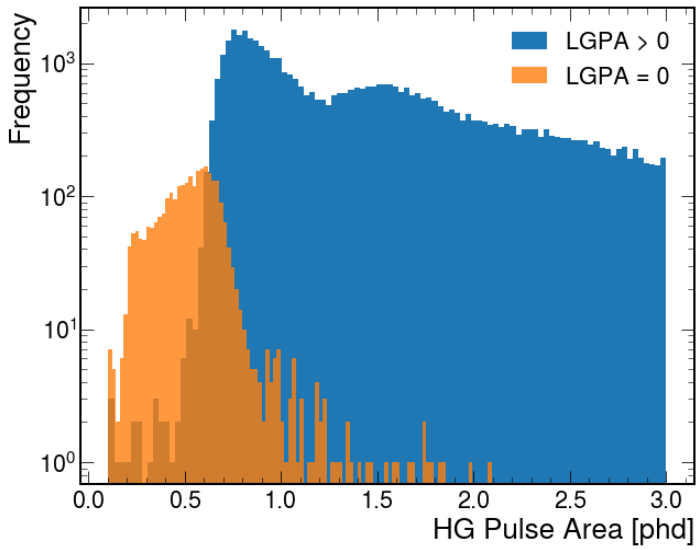

Figure 17: Comparing HG pulse area when a pulse does and does not have an associated LG pulse. HG pulses typically do not have a LG pulse when HGPA < 0.5 phd. LZ does not plan to use the LG channel for pulses with HGPA < 10 phd, so this energy threshold is sufficient.

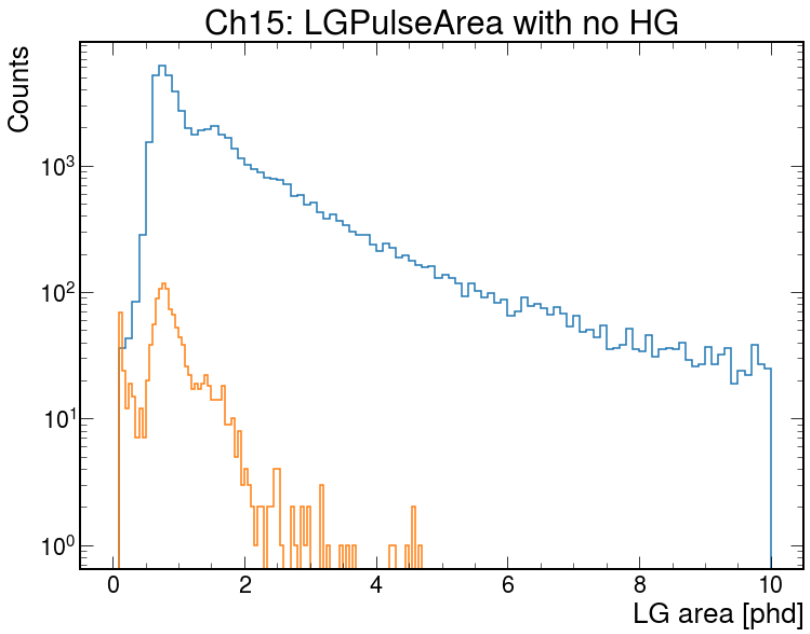

Figure 18: At low pulse areas, LG with no HG should not exist. If a pulse is large enough to be seen in the LG channel, it should certainly be seen in the HG channel. However, a large amount of LG pulses with no HG pair exist in the data (orange). Pulses with both HG and LG are plotted to give reference to how common these abnormalities are (blue).

.

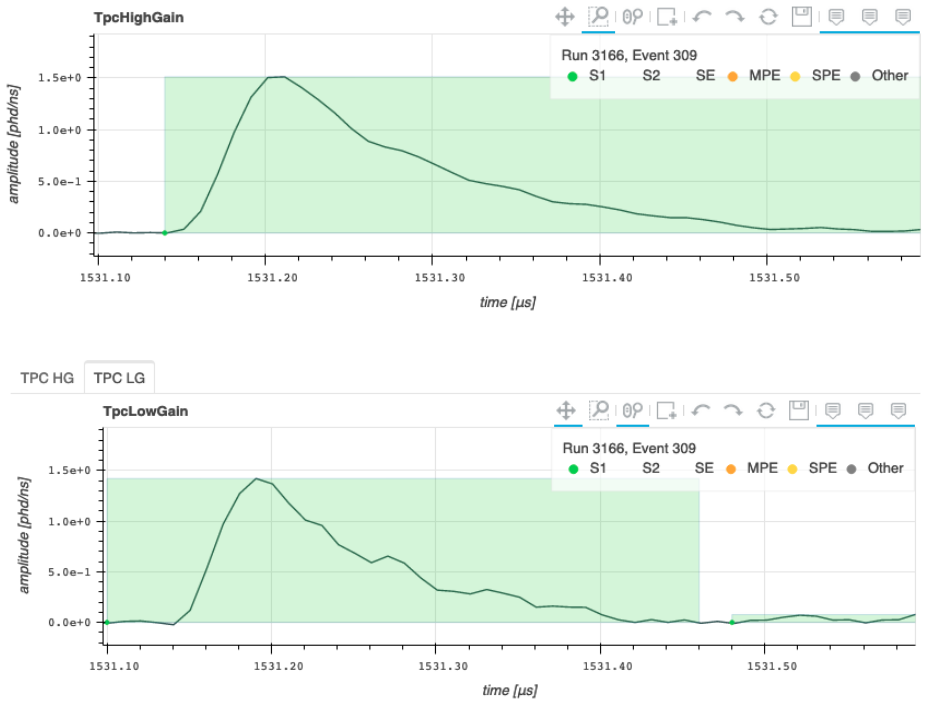

Figure 19: An example of the pulse-finder observing one pulse in the HG channel, but multiple pulses in the LG channel. The second LG pulse would then not have an associated HG pulse.

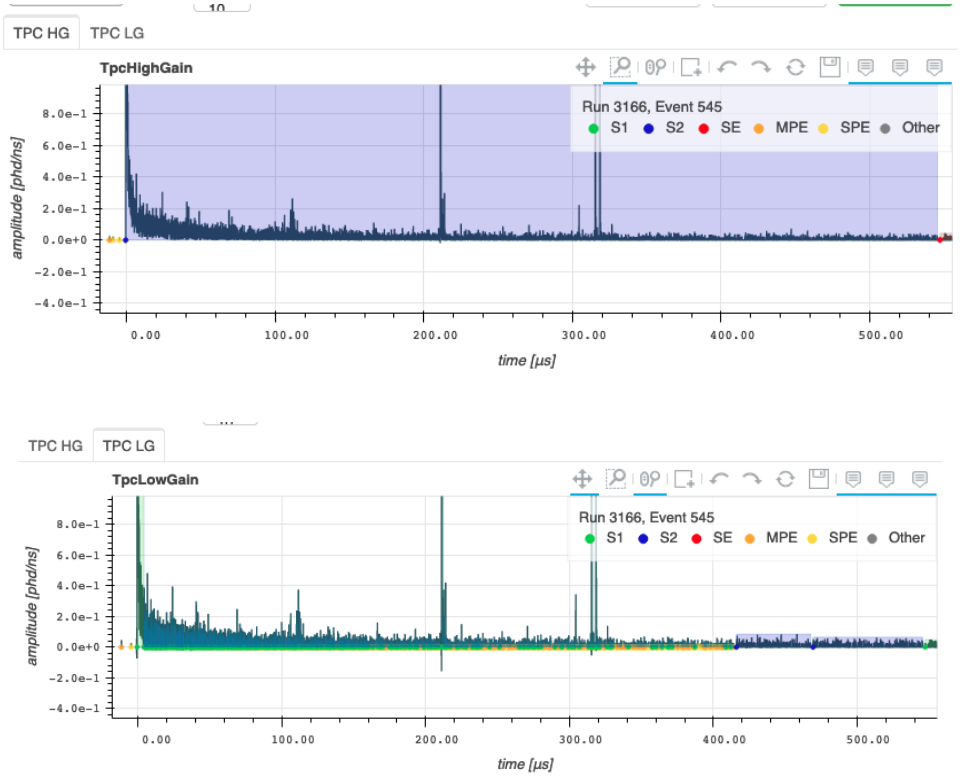

Figure 20: This is an extreme example of the previous figure. One HG pulse was then seen as 1600 LG pulses. These types of pulses will need to be fixed in the pulse-finder for relating HG and LG in the future.

The Future of LZ

The LZ dark matter experiment will be the most sensitive dark matter experiment in the next decade. If dark matter truly consists of WIMPs, LZ is probing deep into that parameter space with a real chance of detecting it. The final preparations for LZ are being made and we hope to start collecting real data very soon. The mixed gain output signals from the TPC PMTs will allow for a more accurate pulse reconstruction, even for otherwise saturated signals. This allows for more accurate calibrations and more trustworthy data collection. As I have shown, the HG and LG pulse areas agree very well for unsaturated data, and still produce an easy-to-use linear trend for saturated data. Some channels will need extra surveillance of their LG channel, and I have listed those for our collaboration. I look forward to seeing what LZ has in store for the future of physics as a whole.

References

[1] F. Zwicky, “Die Rotverschiebung von extragalaktischen Nebeln”, Helv. Phys. Acta 6, 110–127 (1933).

[2] V. Rubin, “Dark Matter in Spiral Galaxies”, Scientific American Vol. 248, No. 6 (June 1983), pp. 96-109.

[3] Leo, M. D. (2018). *Rotation curve of spiral galaxy Messier 33* [Photograph]. Wikipedia.

[4] D. Clowe, et al., “A Direct Empirical Proof of the Existence of Dark Matter,” The Astrophysical Journal, 648, 2 (2006).

[5] NASA. (2006, August 21). NASA Finds Direct Proof of Dark Matter [Photograph].

[6] N. Aghanim, et al., “Planck 2018 Results. VI. Cosmological Parameters,” Astronomy and Astrophysics, 641, A6 (2020). [arXiv: 1807.06209]

[7] CAHN, R. N. (2007). DARK ENERGY TASK FORCE: FINDINGS AND RECOMMENDATIONS. International Journal of Modern Physics D, 16(12b), 2551–2561.

[8] Peccei, R. D., & Quinn, H. R. (1977). CP Conservation in the Presence of Pseudoparticles. Physical Review Letters, 38(25), 1440–1443. [https://doi.org/10.1103/physrevlett.38.1440]

[9] D.S. Akerib et al. (LZ Collaboration), “The LUX-ZEPLIN (LZ) experiment”, Nucl. Instrum. Meth., A 953, 163047 (2020). [arXiv:1910.09124]

[10] B.J. Mount, et al. (LZ Collaboration), “The LUX-ZEPLIN (LZ) Technical Design Report”, (2017). [arXiv: 1703.09144]

[11] D. S. Akerib, et al. (LZ Collaboration), “The LUX-ZEPLIN (LZ) radioactivity and cleanliness control programs,” The European Physical Journal 80, 1044 (2020). [arXiv: 2006.02506] [https://doi.org/10.1142/s0218271807011267]

[12] D. S. Akerib, et al. (LZ Collaboration), “Projected WIMP sensitivity of the LUX-ZEPLIN dark matter experiment,” Phys. Rev. D 101, 052002, (4 March 2020). [arXiv: 1802.06039]

[13] D. S. Akerib, et al. (LZ Collaboration), “Simulations of Events for the LUX-ZEPLIN (LZ) Dark Matter Experiment”, Astroparticle Physics, 125, 102480 (2020). [arXiv: 2001.09363]

[14] SENSE. (n.d.). PMT Principle [Photograph]. Photomultiplier Tubes (PMT).

[https://www.sense-pro.org/lll-sensors/pmt]